Cellulose (2014) 21:4119–4133
DOI 10.1007/s10570-014-0459-0

ORIGINAL PAPER

Surface modification of cellulose microfibrils by periodate oxidation and subsequent reductive amination with benzylamine: a topochemical study

Nathanaël Guigo · Karim Mazeau · Jean-Luc Putaux · Laurent Heux

Received: 25 April 2014 / Accepted: 22 September 2014 / Published online: 17 October 2014

Abstract Never-dried sulfite wood pulp was beaten and subsequently microfibrillated before being submitted to periodate oxidation for various times. The oxidation progress, which was followed by ^{13}C solid-state NMR spectroscopy in conjunction with degree of oxidation (DO) measurements together with ultrastructural observations, revealed that the cellulose crystallinity and microfibrillar integrity were kept intact until a DO of 0.3/0.4, indicating that at that level, the cellulose microfibrils had been oxidized exclusively at their surface. Beyond this DO value, the sample crystallinity started to deteriorate, as the oxidation progressed toward the core of the microfibrils. Remarkably, throughout the oxidation, the created carbonyl moieties were never observed, as they were readily recombined into hemiacetals by cyclization either within the same anhydro glucose unit (AGU) or with the adjacent un-oxidized AGUs of the same cellulose chain. At DO below 0.3/0.4, hemiacetal coupling with adjacent cellulose chains was also considered, but it appeared unlikely in view of the interchain distance imposed by the crystalline lattice. The oxidized samples were subjected to a reductive amination with benzylamine in order to convert their hydrophilic surfaces into hydrophobic ones. Despite the ease of this derivatization, the analysis of the ^{13}C solid-state NMR spectra of the aminated products showed that, below a DO of 0.3, only half of the hemiacetal moieties could be converted into secondary amine products, whereas the other half remained untouched, likely for steric reasons.

Keywords Cellulose microfibrils · Surface modification · Topochemistry · Hemiacetal cyclization · Periodate oxidation · ^{13}C CP-MAS solid-state NMR

N. Guigo · K. Mazeau · J.-L. Putaux · L. Heux
Centre de Recherches sur les Macromolécules Végétales (CERMAV), Université Grenoble Alpes, 38000 Grenoble, France

N. Guigo · K. Mazeau · J.-L. Putaux · L. Heux (✉)
CNRS, CERMAV, 38000 Grenoble, France
e-mail: Laurent.Heux@cermav.cnrs.fr

Present Address:
N. Guigo
Laboratoire Physique de la Matière Condensée, UMR 7336, CNRS, Université Nice Sophia Antipolis, 06100 Nice, France

Introduction

In search for abundant and renewable materials with high performance potential, cellulose microfibrils stand out as prominent candidates (Siro and Plackett 2010; Klemm et al. 2011; Charreau et al. 2013). Their unique properties, which originate from their mode of biosynthesis, reveal that each microfibril is in fact a nanometer-sized slender crystalline rod (Chanzy

1990; Brown 1996; Nishiyama 2009), presenting a high aspect ratio, high elastic modulus and high breaking strength, together with a relatively low density (Moon et al. 2011). To exploit such interesting characteristics fully, intense research programs are being developed to investigate the properties and the potential of microfibrils extracted from purified cellulosic materials (Klemm et al. 2011). The microfibril extraction, normally achieved under aqueous environment, results from specific mechanical disintegration, combined or not with chemical or enzymatic treatments (Turbak et al. 1983; Henriksson et al. 2007; Spence et al. 2011). Once extracted, the microfibrils find many potential applications, the most frequently mentioned being those of fillers for nanocomposites, thickening or gel-forming agents as well as reinforcers for paper and paper boards, but there are many more possibilities in the fields of cosmetics, pharmaceuticals, etc. (Moon et al. 2011; Lavoine et al. 2012; Charreau et al. 2013).

One of the drawbacks to the use of cellulose microfibrils into new products is their high hydrophilicity (Nishiyama 2009), a feature that restricts their processing to being only in aqueous or highly polar media. In order to widen their use into the more common non-polar media, their hydrophilic surface needs to be transformed to acquire a hydrophobic character, while their inner core and therefore their physical characteristics remain intact. Such a surface hydrophobization can be achieved by the addition of selected surfactants, a method that is easy to carry out and that has been shown to promote the dispersion in apolar solvents (Heux et al. 2000) as well as in molten plastic, e.g., polyolefins (Ljungberg et al. 2005, 2006). Similarly, one can take advantage of carbohydrate–carbohydrate interactions to design smart molecules with an anchoring head and a functional tail either after a chemoenzymatic modification of xyloglucan (Brumer et al. 2004) or by sequential adsorption followed by click reaction (Filpponen et al. 2012). As opposed to the adsorbed molecules that are likely to present some lability under certain circumstances, surface covalent bonding is preferred for more permanent hydrophobization or when stress-transfer is needed from the matrix to the particles in the case of nanocomposite preparations. This can be achieved for instance by derivatizing the surface hydroxyl groups by silylation (Goussé et al. 2004), acetylation (Sassi and Chanzy 1995), coupling with isocyanates (Siqueira et al. 2010), cationic functionalization by epoxidation (Hasani et al. 2008), etc. Whereas most of these derivatization protocols are achieved in a solvent environment, gas phase modification, applied to microfibril aerogels (Berlioz et al. 2009; Fumagalli et al. 2013a, b), is a promising method to achieve solvent-free surface hydrophobization. However, the experimental conditions require moderate boiling temperatures for the reagents, which therefore are restricted to moderately bulky molecules.

Modifying cellulose microfibrils by oxidizing the surface hydroxyl groups is an interesting route, which allows the decoration of the microfibril surface with carbonyl or carboxyl groups that are more reactive than the initial primary or secondary alcohols. In this line, the surface oxidation of cellulose microfibrils with NaBr and NaClO mediated by 2,2,6,6-tetramethyl pyridine-1-oxyl (TEMPO) radical (Bragd et al. 2004; Saito and Isogai 2004; Montanari et al. 2005) has been attracting much attention as it has proven high selectivity in the exclusive conversion the cellulose surface hydroxymethyl groups into carboxyls. This surface oxidation has demonstrated a remarkable stabilizing effect to prevent the microfibrils from flocculating when dispersed in aqueous suspensions (Saito et al. 2006). The surface carboxyl groups are prone to coupling with various reagents and in particular with compounds containing primary amine moieties to yield selective surface grafting (Araki et al. 2001; Azzam et al. 2010).

As opposed to the TEMPO oxidation method that keeps the glucosyl rings intact, the periodate oxidation technique involves the opening of the ring and the formation of two aldehyde groups at the C2 and C3 of the anhydro glucose units (AGU), leading to the dialdehyde cellulose (DAC) (Jackson and Hudson 1937; Jackson and Hudson 1938). The opening of the glucosyl ring induces a major increase of the flexibility of the oxidized cellulose chains, as it brings a torsional freedom to the C–C and C–O linkages, which no longer freeze the pyranosyl rings in their initial rigid $^4C_1$ chair shape (Casu et al. 1985). Such an increase in flexibility could explain the observed high wet strength of periodate oxidized paper handsheets (Zeronian et al. 1964) or the unique tensile properties of films and sheets from dialcohol cellulose (Kasai et al. 2014; Larsson et al. 2014). From the chemical point of view, DAC appears to be a highly reactive intermediate that can be further derivatized into

dicarboxylic (Maekawa and Koshijima 1984; Varma et al. 1997; Kim et al. 2000), imine (Maekawa and Koshijima 1991; Kim et al. 2000; Liimatainen et al. 2012), sulfonate (Hou et al. 2007; Zhang et al. 2008), etc. Whereas for the TEMPO oxidation, the conditions to selectively oxidize cellulose microfibril surfaces are well established, such conditions remain to be determined for periodate treated samples. In fact, a study achieved with the periodate oxidation of cellulose whiskers from *Cladophora* has suggested an uneven distribution of the dialdehyde groups (Kim et al. 2000). It is not clear whether such a phenomenon is due to the specific high crystallinity of *Cladophora* cellulose or whether it can be generalized to the more common celluloses. Another important aspect of the preparation of DAC is that the HCO groups that are created on a given pyranosyl residue are likely to react with either the OH groups of adjacent untouched residues (Painter and Larsen 1970) or even with the hydroxymethyl group of the same residue. Other possibilities exist with the hydroxyl moieties of other chains in proximity within the cellulose crystalline lattice. Such reactions lead to the formation of hemiacetal linkages (Ishak and Painter 1971; Potthast et al. 2007), which may slow down the progress of the DAC formation (Ishak and Painter 1971) and therefore are likely to hamper the surface oxidation of the microfibrils. These side reactions explain why the periodate oxidation takes many days to be substantial (Lindh et al. 2014).

Considering the above questions, the goal of the present article was to gain more knowledge on the topochemistry of the surface oxidation of cellulose subjected to the periodate protocol. For this, microfibrils from never-dried wood pulp were oxidized for increasing times, special attention being paid to the low degree of conversion range where only the microfibril surface was expected to be oxidized into DAC, thus keeping the microfibrillar nature of the corresponding samples, as revealed by transmission electron microscopy (TEM). The surface-oxidized DAC microfibrils were then hydrophobized by reductive amination with benzyl amine to yield benzylaminated cellulose (BAC) microfibrils. Both the DAC formation and BAC conversion were followed by quantitative CP-MAS ^{13}C NMR spectroscopy. The analysis of the resulting spectra allows us to monitor the ultrastructural changes (new chemical bonds and crystallinity) as a function of the degree of oxidation (DO), together with the quantization of the degree of substitution (DS) resulting from the benzylamine coupling and the amount of formed hemiacetal. These data provide new insights in the topochemistry of both the periodate oxidation mechanism and the subsequent amination processes, as shown in Scheme 1.

Materials and methods

Materials

Never-dried bleached sulfite hardwood pulp was obtained from Tembec Tartas. The pulp was first beaten for 6 h in a Valley beater, using an aqueous pulp suspension of 2 % (w/w). The resulting beaten pulp was further treated for 45 min with a laboratory scale homogenizer (Manton-Gaulin, type 15MR/31MRfrom APV) operated at 500 bars. The resulting creamy stock suspension, which had a solid content of (2.0 ± 0.05) %, was stored at 4 °C before use.

Sodium metaperiodate, benzylamine and sodium cyanoborohydride were purchased from Aldrich. Hydroxylamine hydrochloride was acquired from

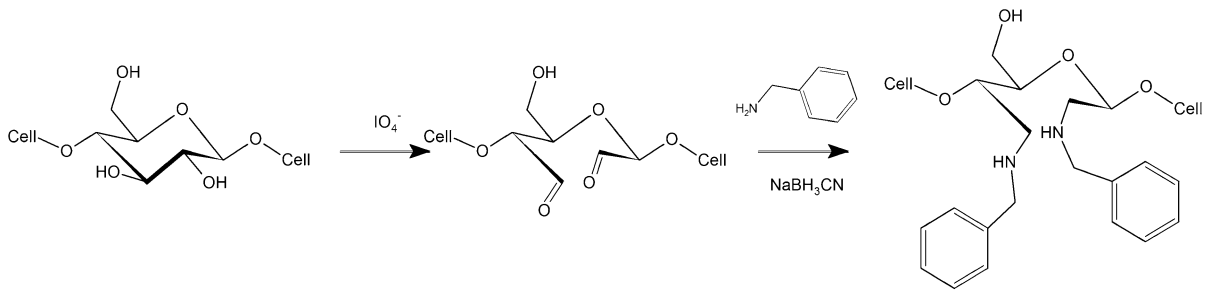

Scheme 1 Reaction scheme of periodate oxidation of cellulose and subsequent coupling with benzylamine

Fluka. All these reagents, which were of analytical grade, were used without further purification.

Preparation of DAC microfibrils by periodate oxidation

In a typical run, 50 mL of stock suspension was exchanged to distilled water by successive centrifugations; the final pellet was diluted to 100 mL in distilled water and vigorously stirred for 20 min. In most runs, 1.72 g of sodium periodate (i.e., 1.3 molar equivalent per AGU) was added to the suspension. In other instances and to highlight the influence of the periodate concentration, some samples were treated with 6.88 g of sodium periodate (i.e., 5.2 molar equivalent per AGU). The mixtures were put into the dark to avoid periodate decomposition (Symons 1955). The oxidation reaction was conducted for various times, ranging from 4 to 67 h, at room temperature (~20 °C) under mechanical stirring. At the end of the reaction, the DAC suspension was centrifuged at 12,000 g for 15 min. The pellet was then re-dispersed into distilled water and recovered by a new centrifugation. Five to six centrifugation/redispersion cycles were then performed to ensure that all the periodate had been washed away: this was checked by verifying that the supernatant of the last centrifugation had a conductivity measurement close to that of distilled water (2 μS cm^{-1}).

After the recovering process, parts of the wet DAC samples were immediately analyzed by ^{13}C solid-state NMR, while other parts were freeze-dried prior to NMR analysis.

Derivatization of DAC by reductive amination

The never-dried DAC microfibrils (about 500 mg on a dry basis) from the last pellet were dispersed into 100 mL of 0.1 M phosphate buffer at pH = 6. Benzylamine (1.32 g) and sodium cyanoborohydride (1.16 g) were added to the suspension. For these two compounds, a large excess was used giving a benzylamine/anhydroglucose (AGU) and cyanoborohydride/AGU molar ratio of 4:1 and 6:1, respectively. The reductive amination was conducted for 24 h at room temperature under mechanical stirring. The resulting BAC microfibrils were recovered by centrifugation and washed two times with distilled water, two times with methanol and again two times with distilled water in order to eliminate the excess of cyanoborohydride and benzylamine. At the end of the washing procedure, the pH and conductivity of filtrate were controlled to ensure that they were in the same range as those of distilled water. The DAC microfibrils were then freeze-dried before characterization.

Carbonyl group content analysis: degree of oxidation (DO)

The carbonyl group content was determined by following the titrimetric method of Zhao and Heindel (1991), which was also recently applied to DAC by Larsson et al. (2008). In this method, each available carbonyl group reacts with hydroxylamine hydrochloride to form an oxime while one proton is released. First, 25 mL of 0.25 M hydroxylamine hydrochloride solution was adjusted to pH 3.2. Then, approximately 100 mg of never-dried DAC microfibrils was added to the solution and stirred for 2 h at room temperature. The reaction mixture was titrated back to pH 3.2 with a standardized 0.01 N NaOH solution. The weight of titrated DAC microfibrils was precisely determined after centrifugation, washing and freeze-drying. A blank titration was achieved with non-oxidized microfibrils from the starting material. The DO was calculated as follows:

$$DO = \left[\left(V_{(NaOH\ sample)} - V_{(NaOH\ blank)}\right) \times C_{NaOH} \times M_{AGU}\right] / m_{DAC(dry\ basis)}$$

where $V_{(NaOH\ sample)}$ and $V_{(NaOH\ blank)}$ are the volume (in mL) of NaOH solution to obtain back titration to pH = 3.2 of respectively DAC and non-oxidized microfibrils, C_{NaOH} is the NaOH concentration (0.01 mol L^{-1}), M_{AGU} is the molecular weight of an anhydroglucose unit (162 g mol^{-1}), and $m_{DAC(dry\ basis)}$ is the weight on a dry basis (in mg) of the titrated DAC sample.

^{13}C CP-MAS solid-state NMR

Solid-state NMR experiments were performed with a Bruker Avance DSX 400 MHz spectrometer operating at 100.6 MHz for ^{13}C, using the combination of the cross-polarization, high-power proton decoupling and magic angle spinning (CP/MAS) method. The spinning speed was set at 12,000 Hz. The ^{1}H radio-frequency field strength was set to give a 90° pulse

duration of 2.5 µs. The ^{13}C radio-frequency field strength was obtained by matching the Hartman-Hahn conditions at 60 kHz. Recording at least 2,000 scans with contact time and recycle delay, respectively, of 2 ms and 2 s represented standard conditions. The acquisition time was set at 35 ms and the sweep width at 29,400 Hz. The spectra were calibrated with respect to the carbonyl peak of glycine, which, as an external standard, was set at 176.03 ppm.

Transmission electron microscopy (TEM)

The various microfibrillar suspensions were diluted with distilled water to reach a concentration of around 0.001 wt%. Drops of these diluted suspensions were deposited on glow-discharged carbon-coated TEM grids and allowed to dry. The specimens were then negatively stained with 2 % uranyl acetate and observed using a Philips CM200 electron microscope operated at 80 kV. Images were recorded on Kodak SO 163 films.

Molecular modeling

A cellulose chain containing seven glucosyl residues was extracted from an equilibrated super-crystal of the Iβ allomorph (Mazeau 2005). This chain was then manually modified with the Material Studio program (Accelerys Inc., San Diego, CA, USA) in order to create the different single chains of modified cellulose (models a–e in Fig. 5). The oxidized chain (model a) was also combined with a native one to generate model f. Each model was optimized with the Universal force field (Rappe et al. 1992) using the conjugate gradient procedure with the convergence criterion of the root-mean square of the atomic derivatives of 0.05 kcal mol^{-1} $Å^{-1}$.

Results and discussion

Reaction kinetics

Figure 1 presents the DO of the various samples, deduced from oxime titration as a function of time. As reported in the literature (Kim et al. 2000; Yang et al. 2013; Lindh et al. 2014), the reaction is rather slow, with a time scale in the order of days: 24 h was typically required to reach a DO of 0.5, and after 72 h, the DO reached only 1 out of 2 if all the AGUs had been oxidized. Beyond 72 h, the oxidation was still proceeding, and no leveling off of the reaction was detected. Interestingly, the kinetics of the reaction seemed to follow two different rates: a first rapid increase from a DO of 0 to 0.3/0.4 and then a slower increase of the carbonyl content indicating a slow tapering off of the oxidation rate.

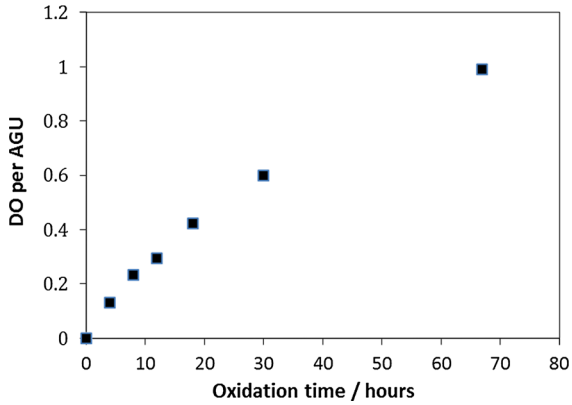

Fig. 1 Evolution with time of the degree of oxidation (DO) per anhydro-glucose unit (AGU)

Analysis of the oxidized never-dried samples

Figure 2 shows the ^{13}C CP-MAS spectra of cellulose microfibrils at different oxidation times, achieved in the never-dried wet state. The spectrum of the unmodified substrate (Spectrum 2a) displays the characteristic resonances of crystalline cellulose between 110 and 50 ppm. It consists of (1) a multiplet at 105 ppm assigned to the C1 carbon of cellulose, (2) two resonances around 88 and 85 ppm assigned respectively to the C4 carbons in ordered and disordered chain, and (3) a similar splitting of the signal arising from the C6 carbons at 65 and 62 ppm, also respectively corresponding to ordered and disordered chains. In addition to these well-characterized signals, a complex cluster between 72 and 68 ppm originates from the overlapping of contributions of the C2, C3 and C5 carbons and remains unresolved. Finally, around 101.5 ppm, there is a small resonance, which corresponds to the presence of leftover hemicelluloses that are still present in the bleached sulfite wood pulp (Newman and Hemmingson 1998). Interestingly, the

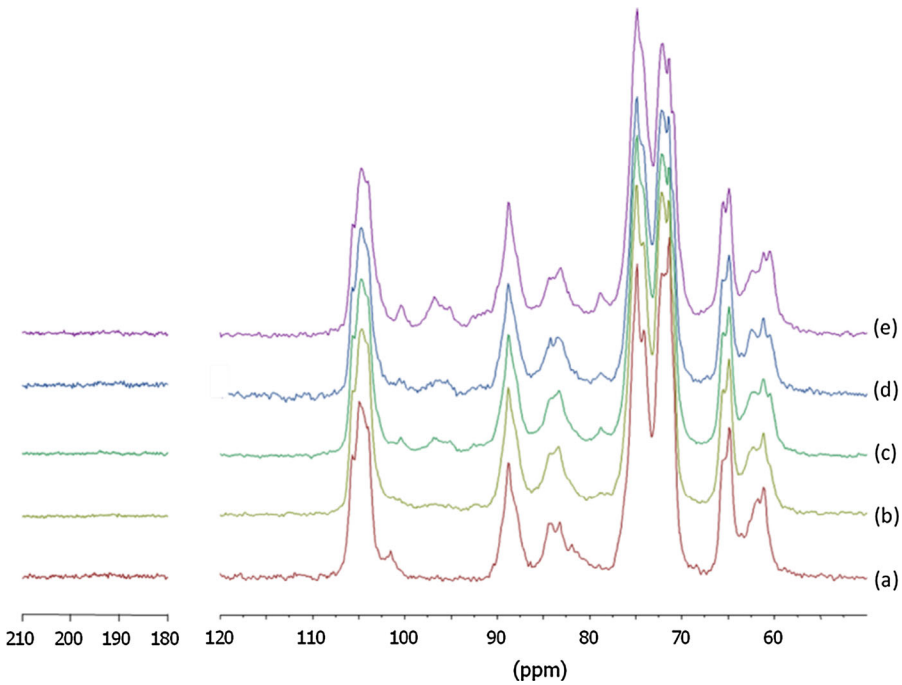

Fig. 2 The ^{13}C CP-MAS NMR spectra in the wet state of (*a*) initial microfibrils and after a periodate oxidation of (*b*) 4 h, (*c*) 8 h, (*d*) 12 h and (*e*) 18 h. (Color figure online)

presence of residual water in these never-dried samples induces a resolution enhancement for the carbons of the non-crystalline cellulose, materialized by the splitting of the signals at 85 and 62 ppm into sharp doublets. Such sharp doublets, first observed in never-dried cotton fibers (Hirai et al. 1990), disappear when the cellulose samples are dried. This splitting has been assigned to two crystallographically different cellulose surfaces (Larsson and Westlund 2005).

Upon oxidation, gradual changes in the spectral features were observed. In this work, the samples that were investigated by solid-state NMR corresponded to a series of oxidized specimens up to 18 h in oxidation time. Beyond this limit, the wet samples could not be measured as they lost their mechanical integrity and therefore could not be handled for solid-state NMR. In the spectra of the oxidized samples shown in Fig. 2 (spectra 2b–2e), the resonance at 100 ppm is absent, indicating a rapid dissolution of the oxidized hemicelluloses. Besides this disappearance, it is remarkable that the spectra of the oxidized specimens do not display any resonance in the carbonyl region (180–210 ppm), despite the extent of the oxidation, which creates two carbonyl groups for each AGU opening. Such absence unambiguously indicates that all the created carbonyl moieties are metastable and thus prone to a rapid recombination. In the spectra shown in Fig. 2, six new peaks at 100.4, 96.8, 95.1, 91.5 (broad) 78.8 and 60.6 ppm, connected with the extent of oxidation, are observed, and their intensity keeps increasing with the oxidation time. Another feature deduced from the spectra in Fig. 2 is that the cellulose part of the spectrum does not seem to be much affected by the oxidation, indicating that the crystallinity of the samples is not much reduced, at least during the first 18 h of oxidation that were considered. In particular, the sharpness of the resonances attributed to crystalline cellulose appears totally unaffected up to 12 h of oxidation (DO = 0.3), and as a consequence, the corresponding samples do not show any hint of decrystallization. Thus, up to this level, the oxidation is essentially located at the surface of the microfibrils, while their microfibrillar crystalline core remains intact. In the present case, the high accessibility of never-dried microfibrils used as starting material is a significant advantage that promotes a uniform surface derivatization of most microfibrils.

Morphology of the never-dried oxidized samples

TEM images of initial and oxidized samples are shown in Fig. 3. When the DO was above 0.4, the suspensions contained aggregates that could not be

sufficiently broken into smaller fragments by gentle homogenization, thus preventing TEM observation. The initial sample (Fig. 3a) mostly consisted of dispersed slender microfibrillar bundles with a length of a few micrometers and a width typically ranging from 20 to 50 nm. This type of bundle is classically observed from microfibrillar cellulose prepared by high-pressure mechanical disruption (Herrick et al. 1983; Moon et al. 2011). As emphasized by the negative staining, each bundle is in fact a rather tight fascicle of individual microfibrils of no more than 3–4 nm in diameter. The sample in Fig. 3b, which corresponds to a DO of 0.2, was relatively similar to the one in Fig. 3a, except that a fraction of shorter bundles and some individual kinked microfibrils were observed. In addition, the bundles appeared to be slightly wider than those in Fig. 3a, indicating that their constituting microfibrils were more separated than in the initial sample, thus giving the impression of slightly swollen bundles. This swelling was drastically more pronounced in the sample shown in Fig. 3c (DO = 0.4). The image shows coexisting organized and disorganized bundles. The diameter of organized bundles is roughly twice as large as those in the initial sample, although their length is similar to what was observed in Fig. 3a, b. Despite this overall swelling, the constituting individual microfibrils, still with their original diameters, are observed, but they tend to exhibit a somewhat segmented aspect. This effect is even clearer along the disorganized microfibrils that are not fasciated into bundles any longer. Many kinks are observed, separated by 100–200 nm-long straight segments. Interestingly, the length of the segments is comparable to the length of the whisker-like nanocrystals obtained after sulfuric acid hydrolysis of cellulose microfibrils (Elazzouzi-Hafraoui et al. 2008), which thus suggests that the amorphous regions of the microfibrils are somehow affected and weakened by the oxidation treatment. In the disorganized bundles, e.g., in the upper left corner of Fig. 3c, individual microfibrils and microfibril fragments are observed, but they are no longer fasciated into slender bundles as in the other part of the micrograph or in Fig. 3a, b. These individual elements are frequently much shorter and often organized into kinked structures. This phenomenon strongly recalls what was observed after TEMPO oxidation for which individualized microfibrils were even observed at the highest oxidation rate

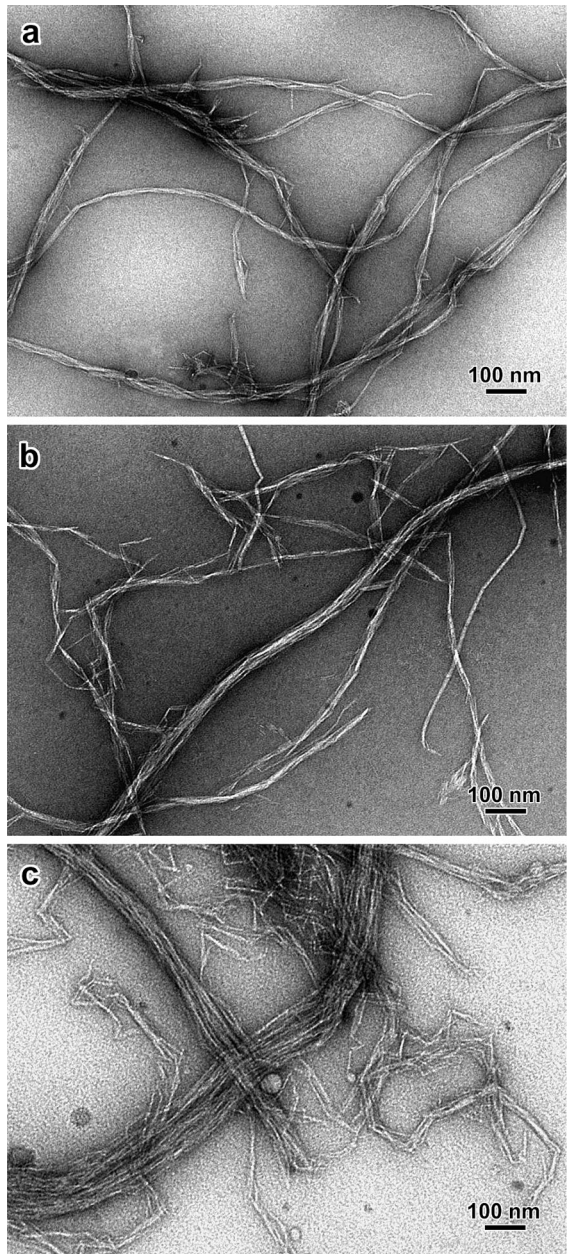

Fig. 3 TEM images of negatively stained cellulose samples: **a** untreated specimen; **b** after a 8 h oxidation (DO = 0.2); **c** after a 16 h oxidation (DO = 0.4)

(Saito et al. 2006). However, one major difference between the two systems is the impossibility of obtaining observable dispersion at the highest DO. In the case of the enhancement of nanofibrillation by a sequential periodate-chlorite oxidation pretreatment of wood cellulose (Liimatainen et al. 2012),

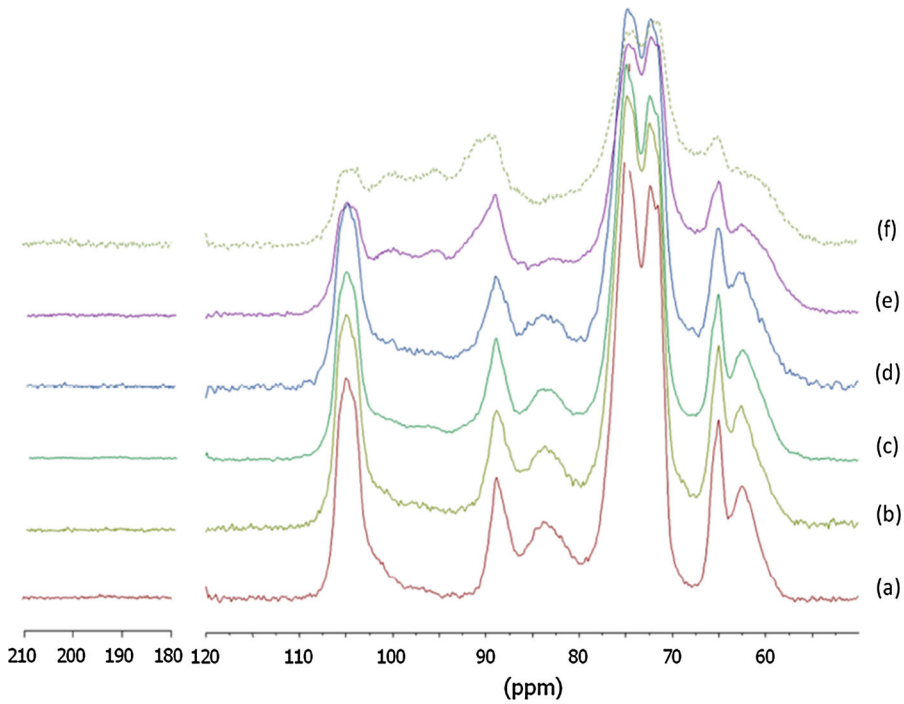

Fig. 4 ^{13}C CP-MAS spectra in the dry state of (*a*) raw microfibrils; after a periodate oxidation of (*b*) 4 h, (*c*) 8 h, (*d*) 12 h, (*e*)18 h and (*f*) 4 h, 4 eq. (Color figure online)

nanofibrils were also observed, but for modest DO (carboxyl contents ranging from 0.38 to 1.75 mmol g^{-1} i.e. DO < 0.3), in excellent agreement with our observations. Similarly, after treating cellulose fibers with a two-step oxidation process involving sodium periodate followed by sodium chlorite, individualized particles with a charge density of 1.4 mmol g^{-1}, i.e., DO ≈ 0.23, were obtained (Yang et al. 2013), indicating a surface charge density compatible with our own observations. Therefore, it seems that the topochemistry of the periodic oxidation reaction is substantially different from that of the TEMPO case.

These observations indicate that at the beginning, the periodate oxidation is essentially a surface derivatization, which does not disturb the microfibrillar nature of cellulose, in line with solid-state NMR results. At a DO of 0.4 and below, the salient effect seems to loosen the microfibrillar bundles by separating the microfibrils from one another. This loosening may be due to oxidation of the amorphous parts located along the microfibrils, therefore inducing some individualization of these elements. More likely, the conversion of surface hydroxyl groups into carbonyl could reduce the cohesion of the microfibrils within the bundles by suppressing the hydrogen bonds that glue the microfibrils into bundles.

Analysis of the oxidized dried samples

Even if the intensity of the extra resonances in the spectra in Fig. 2 regularly increases with the course of the reaction for the substrates oxidized in the never-dried state, it is interesting to investigate what happens with the oxidized samples when dried, since such conditions correspond to the commonly studied cases (Kim et al. 2000; Potthast et al. 2007; Yang et al. 2013; Larsson et al. 2014). Moreover, one of the limitations of the CP-MAS technique with wet substrates is the loss of quantitativeness due to the motional averaging of the dipolar coupling for the most dynamical moieties, thus hampering the polarization transfer during the CP process. For these reasons, freeze-dried samples were also analyzed and their ^{13}C CP-MAS spectra recorded (Fig. 4).

As in the case of the never-dried samples and as already reported by Kim et al. (2000), the spectral features of the oxidized dried samples do not show any hint of carbonyl resonance in the 180–210 ppm region. Besides such an absence, the spectra present a continuous but yet fuzzier evolution with oxidation time. Indeed, even if the typical line shapes of the initial cellulose microfibrils can still be identified, they are progressively overwhelmed by large signals that

more or less blur the appearance of the spectra and render problematic the quantitative analysis of the individual resonances. Such a spectral evolution was already observed by Kim et al. (2000) and was interpreted as the sign of the disruption of the crystalline domains. However, the spectra recorded with the samples oxidized in the wet state (Fig. 2) clearly indicate that the crystallinity of the samples was kept intact at least until a DO of 0.3. Interestingly, the oxidation of microfibrils during 18 h with 1 equivalent of $NaIO_4$ or 4 h and 4 equivalents leads to very similar results, suggesting that the time and the concentration of reactant play a similar role. Compared to the spectra obtained under wet conditions (Fig. 2), the freeze-dried samples showed rather less resolved lines (Fig. 4). This phenomenon is widely observed for cellulosic samples as the drying procedure freezes the molecular motion and induces a concomitant line broadening because of the non-averaged interactions. However, in the spectra shown in Fig. 4, the onset of a broad contribution between 100 and 90 ppm is observed with increasing DO. It corresponds to the broadened and overlapping resonances located at 100.4, 96.8, 95.1 and 91.5 ppm identified in the wet samples. For the two other lines at 78.8 and 60.6 ppm, their contributions most likely merge with the neighboring contributions from the still underivatized components. Taken together with the six new resonances observed in the oxidized never-dried samples in Fig. 2, it is clear that the absent carbonyl signals are replaced by new bands, which denote the recombination of the carbonyl groups into new entities.

Hemiacetal formation

To account for the formation of these new bonds and by looking at the literature data about the periodate oxidation of mono- and polysaccharides, it is known that the production of carbonyl groups in the close vicinity of primary and secondary alcohol moieties invariably results in their rapid recombination into hemiacetals (Guthrie 1961; Painter and Larsen 1970; Ishak and Painter 1971; Potthast et al. 2005; Perlin 2006). In the case of simple 5- and 6-carbon sugars, this well-described interaction systematically occurs and transforms linear sugars into pyranose or furanose ringed structures, cyclized with a hemiacetal function at their anomeric end (Pigman and Horton 1972). The formation of these hemiacetal groups has been recently revealed by 2D-NMR COSY and HMQC experiments in the case of the periodate oxidation of the soluble polysaccharide dextran (Maia et al. 2011).

In the present case, the condensation of the carbonyl resulting from the oxidation (Fig. 5a) with adjacent alcohol functions likely occurs, leading to specific hemiacetal rings if the carbonyl reacts with an OH group located on the same cellulose chain or a linear hemiacetal if the coupling is with an adjacent chain. When looking at the conformation of a cellulose chain at the surface of a cellulose crystal, possible hemiacetal cyclization involving the created carbonyls at C2 and C3 of a given AGU is expected to occur with the hydroxymethyl moieties of the adjacent AGU units. This reaction leads to seven-member fused rings located toward the chain reducing end and an eight-member one toward the chain non-reducing end (Fig. 5b). Other likely possibilities, already hypothesized in the case of periodate oxidized xylan (Painter and Larsen 1970), involve the coupling of the created carbonyls at C3 with the OH at C2 of the adjacent AGU residue located toward the reducing end and that of the carbonyls at C2 with the C3 of the adjacent AGU residue toward the non-reducing end (Fig. 5c). In both cases, pyranose-like hemiacetal fused rings with a chair conformation are created, which likely prevent further oxidation by blocking the secondary OHs of the two nearest neighbors of the oxidized AGUs. This protection is probably responsible for the observed rapid slowing down of the overall oxidation kinetics. Following such a scheme and when the oxidation progresses, most intact AGUs will become engaged in hemiacetal linkages on both sides, thus bringing the rate of oxidation to a lower limit. Indeed, the opening of these rather stable hemiacetal linkages is required to allow a further oxidation of the intact AGU. Other intra-chain couplings may involve the cyclization of the C3 carbonyl with the hydroxymethyl group of the same AGU residue to yield a five-member cyclic hemiacetal (Fig. 5d) or the cyclization of the carbonyl at C2 with the hydroxymethyl group of the same AGU to yield a six-member cyclic hemiacetal (Fig. 5e). In addition to the formation of these intra-chain hemiacetals, inter-chain connections could also be envisaged, but their existence is unlikely because of the inter-chain distances imposed by the underlying crystalline lattice, at least as far as the microfibril crystalline core remains intact. In line with data on

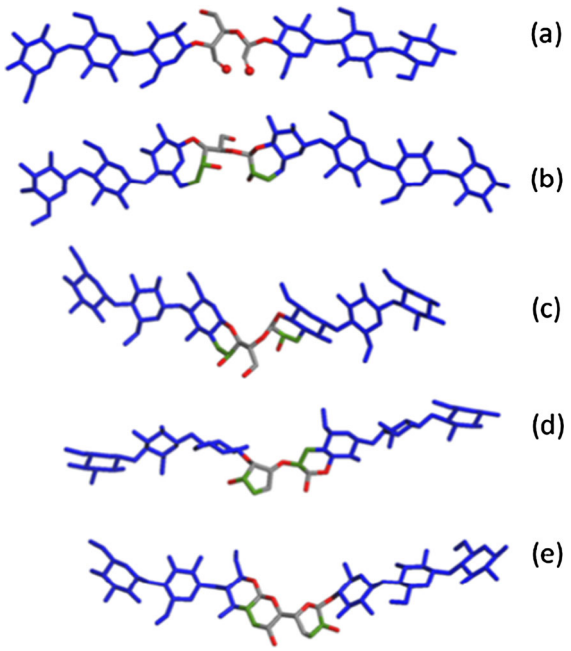

Fig. 5 Model of carbonyl opening and intra-chain hemiacetal reorganizations: (**a**) opening at C2 and C3 of a given AGU unit; hemiacetal cyclization bond at (**b**) C2–O–C6′ (7-member fused ring) and C3–O–C6″ (8-member fused ring); (**c**) C2–O–C3′ (6-member fused ring) and C3–O–C2″ (6-membered fused ring); (**d**) C3–O–C6 (5-membered ring;) for the carbonyl at C2, the cyclization is as in Fig. 3c; (**e**) C2–O–C6 (6-membered ring); for the carbonyl at C3, the cyclization is as in Fig. 3c. The newly formed hemiacetal moieties are colored in *green*. The ring toward the reducing end is labeled with a prime symbol (′), whereas that toward the non-reducing end is labeled with a double prime symbol (″). (Color figure online)

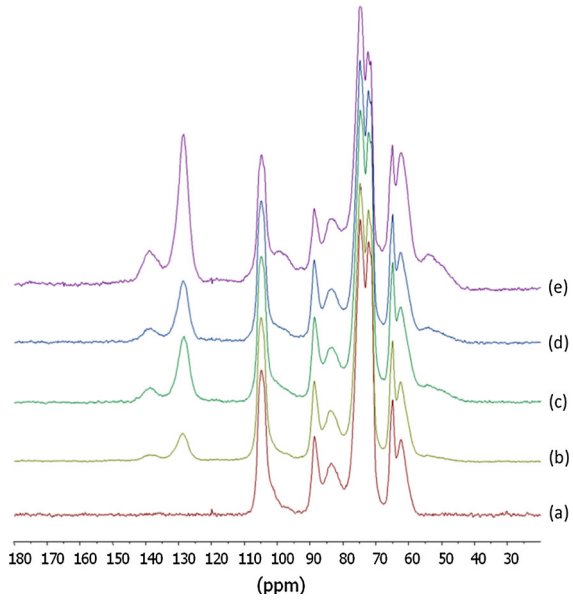

Fig. 6 The ^{13}C CP-MAS spectra in the dry state of benzylaminated microfibrils: (*a*) raw microfibrils; (*b*) from the sample oxidized for 4 h; (*c*) from the sample oxidized for 8 h; (*d*) from the sample oxidized for 12 h; (*e*) from the sample oxidized for 18 h. (Color figure online)

molecular weight determination of variously oxidized cotton samples (Potthast et al. 2007), it is likely that the percentage of intra-chain hemiacetal linkages will be at least dominant at low DO, thus keeping the molecular weight similar to that of the starting microfibrils. At higher DO, when the microfibrils start to be disorganized, the percentage of inter-chain linkages may become substantially higher with a concomitant increase of molecular weight.

When looking at the models presented in Fig. 5b–e, the result of the oxidation followed by the formation of hemiacetals induces some flexibility in the oxidized chain in the cases Fig. 5b, c since the still closed AGU rings become separated by three freely rotating bonds. This increased mobility, which is an interesting asset of the periodate oxidation of cellulose, could account for the observed superior physical properties (Kasai et al. 2014; Larsson et al. 2014) of the oxidized substrates when they are reduced to the dialcohol products to be processed or even of the DAC specimens themselves as stated in earlier studies (Zeronian et al. 1964).

The observed evolution of the spectra for both the wet and dried samples (Figs. 2, 4) is compatible with the above description of possible linkages. First, the creation of hemiacetal cyclization of the carbonyl groups with the neighboring hydroxymethyl moieties (Fig. 5b) will be followed by the appearance of new hemiacetal signals, usually observed between 90 and 100 ppm, and the shift of the C6 signal to higher chemical shifts, as in the case of 1–6 linkages. From a spectroscopic point of view, the situation is rather similar for the cyclic hemiacetal formation described in Fig. 5d, e, for which new hemiacetal linkages are formed that involve a hydroxymethyl unit. Finally, the adjacent cyclization described in Fig. 5c will also create new hemiacetal linkages and most likely will modify the C4 signal by disrupting the O3–O5 intrachain hydrogen bond, probably accounting for the new contribution around 78.8 ppm. However, in view of the great number of possibilities arising from the rearrangement linked to the hemiacetal formation,

it appears difficult to firmly identify a given contribution, but every possibility is likely to happen to an extent that has to be further clarified.

Benzyl aminated samples

When the never-dried oxidized samples were subjected to a reductive amination coupling with an excess of benzylamine, benzylaminated products were obtained after the transient formation of imines products. The solid-state ^{13}C NMR spectra, obtained after purification of the products and subsequent drying, are displayed in Fig. 6.

Compared to the oxidized samples, the BAC microfibrils exhibit three new peaks indicated by dashed lines, presenting increased intensities as a function of the DO of the oxidized samples. Two resonances at 128 ppm and 139 ppm are detected originating from respectively the protonated and quaternary carbon of the benzyl ring of the coupling agent. In addition, a wide contribution appearing near 55 ppm also keeps growing with the DO of the oxidized samples subjected to benzylamination. This signal is typical of the CH_2 group next to a secondary amine resulting from the reductive amination process. Its presence is a direct proof of the covalent coupling of the oxidized samples with benzylamine. Indeed, if a non-covalent interaction of this reagent has taken place, the CH_2 group of its primary amine should resonate around 45 ppm and not at the observed 55 ppm, typical of secondary amines. More strikingly in Fig. 6, one notices that the intensity of the signals between 100 and 90 ppm assigned to the hemiacetal linkages has noticeably diminished after the coupling with benzylamine, indicating that at least part of the hemiacetal groups is readily converted during the reductive amination process. Another important aspect of the spectra shown in Fig. 6 is that the spectral features arising from the cellulosic backbone between 60 and 110 ppm seem unaffected, at least with the samples that had been oxidized up to 12 h. For samples beyond this time, a small but noticeable increase of the disordered contribution to the C4 and C6 signals at around 84 and 62 ppm respectively can be detected in the benzylaminated products.

These observations can be related to the specific aspects of the oxidation and subsequent reductive amination features. The readily formed imine linkages are labile and can be further converted into the secondary amine, but they require at least the presence of a carbonyl group, whereas only hemiacetal bonds have been detected by ^{13}C CP-MAS NMR. This is not so surprising as it has been extensively reported that the reducing ends of polysaccharides—chemically equivalent to the present hemiacetals—can be readily derivatized with a reaction scheme adapted to the reactivity of free aldehydes, which are the minor but still existing form of the hemiacetal linkage. (Hieta et al. 1984; Koyama et al. 1997).

To go further into quantitative details of the spectra shown in Fig. 6, the different contributions arising from the different resonances have been quantitatively evaluated by integration of the respective signals normalized with respect to the area of the C1 peak. Four different types of contributions have been evaluated: (1) that of the C4 peak assigned to the native crystalline cellulose between 86 and 92 ppm, (2) of the CH_2 next to the secondary amines between 46 and 58 ppm, (3) of the carbons from the benzyl ring contributions between 120 and 145 ppm and finally (4) of the carbon engaged in the hemiacetal linkage between 92 and 100 ppm. In Fig. 7, the areas under these peaks have been plotted against the sample DO measured by oxime titration. The integral between 89 and 92 ppm assigned to the crystalline part of the C4 signal is representative of the crystalline core contribution of the cellulose microfibrils that can be defined as a crystallinity index (Heux et al. 1999). Its measured integral remains constant, around 0.42, a value that is classical for wood pulp (Fumagalli et al. 2013a), up to samples presenting a DO of 0.3 corresponding to 12 h of oxidation prior to the reductive amination reaction. Thus, at this level, only the surface of the microfibrils appears modified, whereas their crystalline core remains intact, as observed in the case of surface gas-phase palmitoylation of aerogels of microfibrillated wood pulp (Fumagalli et al. 2013a). In the present case, it is only with samples oxidized for more than 12 h ($DO > 0.3$) that the crystallinity index slightly decreases, which is a sign of a beginning of decrystallization. For much higher DO (data not shown), the crystalline contribution cannot be measured as the native cellulose has been completely destroyed and the corresponding signals merged with those of the amorphous components. These spectroscopic data agree perfectly with the TEM images showing that the morphology drastically changes for DOs between 0.2 and 0.4. The results are also in line

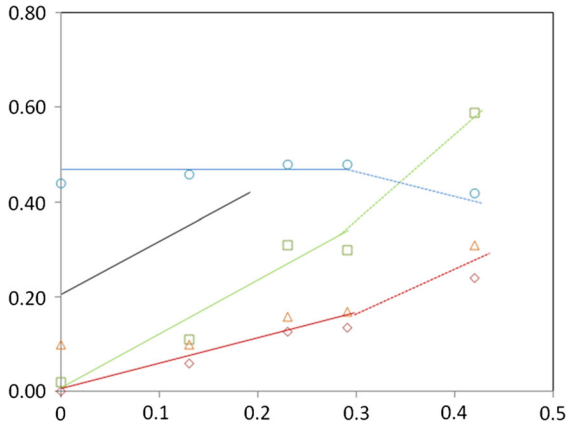

Fig. 7 Normalized integrals of cellulose C4 crystalline contribution (*circles*), CH_2 next to the primary amines (*square*), benzyl ring carbons divided by 6 (*diamonds*) and the carbon atoms involved in the hemiacetal linkages (*triangles*). The lines are not fits but guide the eye; the *dashed line* is a *straight line* of slope 1. (Color figure online)

with the observation by SEM of nanofibrils after a sequential periodate-chlorite oxidation for DO < 0.3 (Liimatainen et al. 2012).

The contributions of the CH_2 groups next to the primary amine and those from the phenyl ring (divided by 6, which is the number of carbons in the benzyl ring) have also been reported in Fig. 7. A first inspection of the graph evidences two regimes that can be distinguished by the evolution of each contribution with the DO. A first one, up to a DO of 0.3, can be described as a linear behavior of each contribution, whereas in a second one, a change in slope is observed above this DO. Other important information is the linear evolution of both the CH_2 next to the amines and the contribution of the carbons of the benzyl rings with a slope of 1 and 0.5 respectively up to a DO of 0.3. This is rather unexpected as the substitution with benzylamines on each aldehyde formed during the oxidation process should lead to the coupling of two benzyl groups per oxidized AGU, and then slope values of 2 and 1 should be observed for a full derivatization. The fact that these slopes are only of 1 and 0.5 most probably indicates that only one of the two available aldehydes is accessible for the reductive amination process. Interestingly, the contribution of the carbon engaged in the hemiacetal linkage, between 92 and 100 ppm, also presents an increase with that of the DO, with the same slope as that of the carbons of the benzyl rings.

The most obvious interpretation of these observations is that one over two (which is the maximum obtainable degree oxidation) of the formed aldehydes per AGU is coupled with benzylamines through the reductive amination process, whereas the other group remains engaged in a hemiacetal linkage until a DO of 0.3. Most probably the steric hindrance related to the vicinity of the crystalline core prevents the coupling with a second benzyl amine molecule when a first one is already coupled. The second aldehyde then has no other option than that of remaining in a hemiacetal bond, as observed for the freshly oxidized samples. This conclusion is in line with the liquid state 2D-NMR spectroscopy data regarding the oxidation of soluble dextran, further modified by *tert*-butyl carbazate (Maia et al. 2011). In this particular case, the authors have shown that 1 out of 2 aldehyde moieties could be converted to carbazone, the second one remaining engaged in a hemiacetal with proximal hydroxyl.

When the DO exceeds 0.3, the full derivatization of both aldehyde groups appears to be possible. Interestingly, the 0.3 value corresponds to the limit beyond which the disruption of the crystalline core of the cellulose substrate starts to take place, as observed in other solid-state derivatizations of cellulose. This is the case for the acetylation of cellulose nanocrystals (Cavaillé et al. 1997) or the gas phase palmitoylation of cellulose microfibrils or nanocrystals with fatty acyl chloride (Fumagalli et al. 2013a, b). As in this latter case, the present oxidized chains are not likely solubilized in the reaction medium, as benzylated cellulosic chains are too hydrophobic to be soluble in water. This is rather different from the acetylation process for which a stripping of the chain is observed as the reaction proceeds with fully acetylated cellulose being soluble in acetic acid. Interestingly, 0.3 is also the DO value for which a change in the oxidation kinetics has been observed. Most probably, the chains that are not directly accessible from the surface are obviously less reactive and should require longer times to be oxidized.

The periodate oxidation of cellulose microfibrils then appears to be a process that is restricted to the surface at least in the first stage of the reaction before the disruption of the cellulose crystalline core. Compared to previous studies in the literature, the peculiarity of the present approach is the use of microfibrillated cellulose and its conservation in a

non-aggregated state by working on never-dried samples. Indeed, most of the drying procedures result in the collapse of the initially separated microfibril bundles into more or less aggregated structures (Fumagalli et al. 2013a). For such collapsed structures, the full accessibility of the samples to the reagents can obviously be drastically impeded, resulting in very different oxidation processes. The preservation of the native microfibrillar structure of the substrate allows a full derivatization of the surface, provided that the modified chains are not soluble in the reaction medium.

Conclusions

The periodate oxidation of cellulose, whereby the glucopyranosyl rings are selectively opened at C2 and C3 and the attached secondary alcohol moieties converted into carbonyl groups, is still a complex and somewhat mysterious process. Indeed, in its study, the ^{13}C solid-state NMR spectra recorded on never-dried microfibrillated cellulose from sulfite wood pulp do not reveal any trace of the expected created carbonyl groups despite the extent of the oxidation. This absence clearly indicates that these groups are readily and entirely recombined into hemiacetals in a coupling reaction with the nearby hydroxyl groups. This reaction likely yields intra- or inter-hemiacetal linkages, depending on whether the coupling is formed along the same or adjacent cellulose chains. The presence of these entities were clearly revealed by the occurrence of at least six NMR resonances whose intensity increases with increasing DO of the samples, indicative of several different hemiacetal configurations. Another salient result of the study is that upon moderate oxidation—up to a DO of 0.3/0.4—the crystallinity and the microfibrillar ultrastructure of the samples were kept intact, showing that the oxidation and therefore the production of hemiacetal surface derivatives was only performed at the cellulose microfibril surface, leaving their core unaffected. The steric hindrance arising from the presence of the hemiacetal linkages could be related to the initial slow kinetics of the reaction and its further slowing down at higher DOs.

When the oxidized samples were subjected to a reductive amination with benzyl amine, part of the hemiacetal groups were readily aminated, yielding a secondary amine coupled with phenyl groups at C2 and C3 of the AGUs. Such a coupling was confirmed by the analysis of the ^{13}C NMR spectra of the aminated samples, where the covalent bond between the coupling and the benzyl ring could be easily identified. In the oxidized samples with DO $= 0.3$ and below, the benzyl amination was effective essentially at the microfibril surface, but only half of the hemiacetals were converted to amines, the other half remaining intact, likely because of steric hindrance.

This study shows that the periodate oxidation of cellulose is a promising derivatization method that, we think, is fairly versatile, provided that the cellulose substrate is adequately prepared and the reaction properly monitored. When the oxidation is limited to the surface of the substrate, the produced hemiacetal groups can serve as a platform for subsequent coupling with other surface reactions.

Acknowledgments The authors thank H. Chanzy for fruitful discussions during the writing of this work, as well as C. Lancelon-Pin for her assistance in the TEM observation of the cellulose samples.

References

Araki J, Wada M, Kuga S (2001) Steric stabilization of a cellulose microcrystal suspension by poly(ethylene glycol) Grafting. Langmuir 17:21–27

Azzam F, Heux L, Putaux J-L, Jean B (2010) Preparation by grafting onto, characterization, and properties of thermally responsive polymer-decorated cellulose nanocrystals. Biomacromolecules 11:3652–3659

Berlioz S, Molina-Boisseau S, Nishiyama Y, Heux L (2009) Gas-phase surface esterification of cellulose microfibrils and whiskers. Biomacromolecules 10:2144–2151

Bragd PL, van Bekkum H, Besemer AC (2004) TEMPO-mediated oxidation of polysaccharides: survey of methods and applications. Top Catal 27:49–66

Brown RM Jr (1996) The biosynthesis of cellulose. J Macromol Sci Pure Appl Chem A33:1345–1373

Brumer H III, Zhou Q, Baumann MJ, Carlsson K, Teeri TT (2004) Activation of crystalline cellulose surfaces through the chemoenzymatic modification of xyloglucan. J Am Chem Soc 126:5715–5721

Casu B, Naggi A, Torri G, Allegra G, Meille SV, Cosani A, Terbojevich M (1985) Stereoregular acyclic polyalcohols and polyacetates from cellulose and amylose. Macromolecules 18:2762–2767

Cavaillé J-Y, Chanzy H, Fleury E, Sassi J-F (1997) Surface-modified cellulose microfibrils, method for making same, and use thereof as a filler in composite materials. PCT Int Appl, WO 9712917

Chanzy H (1990) Aspects of cellulose structure. In: Kennedy JF, Phillips GO, Williams PA (eds) Cellulose sources and

exploitation. Industrial utilization biotechnology and physico-chemical properties. Ellis Horwood Ltd., Chichester, pp 3–12

Charreau H, Foresti ML, Vazquez A (2013) Nanocellulose patents trends: a comprehensive review on patents on cellulose nanocrystals, microfibrillated and bacterial cellulose. Recent Pat Nanotechnol 7:56–80

Elazzouzi-Hafraoui S, Nishiyama Y, Putaux J-L, Heux L, Dubreuil F, Rochas C (2008) The shape and size distribution of crystalline nanoparticles prepared by acid hydrolysis of native cellulose. Biomacromolecules 9:57–65

Filpponen I, Kontturi E, Nummelin S, Rosilo H, Kolehmainen E, Ikkala O, Laine J (2012) Generic method for modular surface modification of cellulosic materials in aqueous medium by sequential click reaction and adsorption. Biomacromolecules 13:736–742

Fumagalli M, Ouhab D, Molina-Boisseau S, Heux L (2013a) Versatile gas-phase reactions for surface to bulk esterification of cellulose microfibrils aerogels. Biomacromolecules 14:3246–3255

Fumagalli M, Sanchez F, Molina-Boisseau S, Heux L (2013b) Gas-phase esterification of cellulose nanocrystal aerogels for colloidal dispersion in apolar solvents. Soft Matter 9:11309–11317

Goussé C, Chanzy H, Cerrada ML, Fleury E (2004) Surface silylation of cellulose microfibrils: preparation and rheological properties. Polymer 45:1569–1575

Guthrie RD (1961) "Dialdehydes" from the periodate oxidation of carbohydrates. Adv Carbohydr Chem 16:105–158

Hasani M, Cranston ED, Westman G, Gray DG (2008) Cationic surface functionalization of cellulose nanocrystals. Soft Matter 4:2238–2244

Henriksson M, Henriksson G, Berglund LA, Lindström T (2007) An environmentally friendly method for enzyme-assisted preparation of microfibrillated cellulose (MFC) nanofibers. Eur Polym J 43:3434–3441

Herrick FW, Casebier RL, Hamilton JK, Sandberg KR (1983) Microfibrillated cellulose: morphology and accessibility. J Appl Polym Sci Appl Polym Symp 37:797–813

Heux L, Dinand E, Vignon MR (1999) Structural aspects in ultrathin cellulose microfibrils followed by ^{13}C CP-MAS NMR. Carbohydr Polym 40:115–124

Heux L, Chauve G, Bonini C (2000) Nonflocculating and chiral-nematic self-ordering of cellulose microcrystals suspensions in nonpolar solvents. Langmuir 16:8210–8212

Hieta K, Kuga S, Usuda M (1984) Electron staining of reducing ends evidences a parallel-chain structure in Valonia cellulose. Biopolymers 23:1807–1810

Hirai A, Horii F, Kitamaru R, Tsuji W (1990) CP/MAS carbon-13 NMR study of never-dried cotton fibers. J Polym Sci Part C Polym Lett 28:357–361

Hou QX, Liu W, Liu ZH, Bai LL (2007) Characteristics of wood cellulose fibers treated with periodate and bisulfite. Ind Eng Chem Res 46:7830–7837

Ishak MF, Painter T (1971) Formation of interresidue hemiacetals during the oxidation of polysaccharides by periodate ion. Acta Chem Scand 25:3875–3877

Jackson EL, Hudson CS (1937) Application of the cleavage type of oxidation by periodic acid to starch and cellulose. J Am Chem Soc 59:2049–2050

Jackson EL, Hudson CS (1938) Structure of the products of the periodic acid oxidation of starch and cellulose. J Am Chem Soc 60:989–991

Kasai W, Morooka T, Ek M (2014) Mechanical properties of films made from dialcohol cellulose prepared by homogeneous periodate oxidation. Cellulose 21:769–776

Kim U-J, Kuga S, Wada M, Okano T, Kondo T (2000) Periodate oxidation of crystalline cellulose. Biomacromolecules 1:488–492

Klemm D, Kramer F, Moritz S, Lindstrom T, Ankerfors M, Gray D, Dorris A (2011) Nanocelluloses: a new family of nature-based materials. Angew Chem Int Ed Engl 50:5438–5466

Koyama M, Helbert W, Imai T, Sugiyama J, Henrissat B (1997) Parallel-up structure evidences the molecular directionality during biosynthesis of bacterial cellulose. Proc Natl Acad Sci USA 94:9091–9095

Larsson PT, Westlund PO (2005) Line shapes in CP/MAS ^{13}C NMR spectra of cellulose I. Spectrochim Acta Part A 62A:539–546

Larsson PA, Gimaaker M, Waagberg L (2008) The influence of periodate oxidation on the moisture sorptivity and dimensional stability of paper. Cellulose 15:837–847

Larsson PA, Berglund LA, Wagberg L (2014) Highly ductile fibres and sheets by core-shell structuring of the cellulose nanofibrils. Cellulose 21:323–333

Lavoine N, Desloges I, Dufresne A, Bras J (2012) Microfibrillated cellulose—its barrier properties and applications in cellulosic materials: a review. Carbohydr Polym 90:735–764

Liimatainen H, Visanko M, Sirvio JA, Hormi OEO, Niinimaki J (2012) Enhancement of the nanofibrillation of wood cellulose through sequential periodate-chlorite oxidation. Biomacromolecules 13:1592–1597

Lindh J, Carlsson DO, Stromme M, Mihranyan A (2014) Convenient one-pot formation of 2,3-dialdehyde cellulose (DAC) beads via periodate oxidation of cellulose in water. Biomacromolecules 15:1928–1932

Ljungberg N, Bonini C, Bortolussi F, Boisson C, Heux L, Cavaillé JY (2005) New nanocomposite materials reinforced with cellulose whiskers in atactic polypropylene: effect of surface and dispersion characteristics. Biomacromolecules 6:2732–2739

Ljungberg N, Cavaillé JY, Heux L (2006) Nanocomposites of isotactic polypropylene reinforced with rod-like cellulose whiskers. Polymer 47:6285–6292

Maekawa E, Koshijima T (1984) Properties of 2,3-dicarboxy cellulose combined with various metallic ions. J Appl Polym Sci 29:2289–2297

Maekawa E, Koshijima T (1991) Preparation and structural consideration of nitrogen-containing derivatives obtained from dialdehyde celluloses. J Appl Polym Sci 42:169–178

Maia J, Carvalho RA, Coelho JFJ, Simoes PN, Gil MH (2011) Insight on the periodate oxidation of dextran and its structural vicissitudes. Polymer 52:258–265

Mazeau K (2005) Structural micro-heterogeneities of crystalline Iβ-cellulose. Cellulose 12:339–349

Montanari S, Roumani M, Heux L, Vignon MR (2005) Topochemistry of carboxylated cellulose nanocrystals resulting from TEMPO-mediated oxidation. Macromolecules 38:1665–1671

Moon RJ, Martini A, Nairn J, Simonsen J, Youngblood J (2011) Cellulose nanomaterials review: structure, properties and nanocomposites. Chem Soc Rev 40:3941–3994

Newman RH, Hemmingson JA (1998) Interactions between locust bean gum and cellulose characterized by carbon-13 NMR spectroscopy. Carbohydr Polym 36:167–172

Nishiyama Y (2009) Structure and properties of the cellulose microfibril. J Wood Sci 55:241–249

Painter TJ, Larsen B (1970) Transient hemiacetal structures formed during the periodate oxidation of xylan. Acta Chem Scand 24:2366–2378

Perlin AS (2006) Glycol-cleavage oxidation. Adv Carbohydr Chem Biochem 60:183–250

Pigman W, Horton D (1972) Structure and sterochemistry of the monosaccharides. In: Pigman W, Horton D (eds) The carbohydrates, chemistry and biochemistry, vol IA, 2nd edn. Academic Press, New York, pp 1–65

Potthast A, Rosenau T, Kosma P, Saariaho A-M, Vuorinen T (2005) On the nature of carbonyl groups in cellulosic pulps. Cellulose 12:43–50

Potthast A, Kostic M, Schiehser S, Kosma P, Rosenau T (2007) Studies on oxidative modifications of cellulose in the periodate system: molecular weight distribution and carbonyl group profiles. Holzforschung 61:662–667

Rappe AK, Casewit CJ, Colwell KS, Goddard WA III, Skiff WM (1992) UFF, a full periodic table force field for molecular mechanics and molecular dynamics simulations. J Am Chem Soc 114:10024–10035

Saito T, Isogai A (2004) TEMPO-mediated oxidation of native cellulose. The effect of oxidation conditions on chemical and crystal structures of the water-insoluble fractions. Biomacromolecules 5:1983–1989

Saito T, Nishiyama Y, Putaux J-L, Vignon M, Isogai A (2006) Homogeneous suspensions of individualized microfibrils from TEMPO-catalyzed oxidation of native cellulose. Biomacromolecules 7:1687–1691

Sassi J-F, Chanzy H (1995) Ultrastructural aspects of the acetylation of cellulose. Cellulose 2:111–127

Siqueira G, Bras J, Dufresne A (2010) New process of chemical grafting of cellulose nanoparticles with a long chain isocyanate. Langmuir 26:402–411

Siro I, Plackett D (2010) Microfibrillated cellulose and new nanocomposite materials: a review. Cellulose 17:459–494

Spence KL, Venditti RA, Rojas OJ, Habibi Y, Pawlak JJ (2011) A comparative study of energy consumption and physical properties of microfibrillated cellulose produced by different processing methods. Cellulose 18:1097–1111

Symons MCR (1955) Evidence for formation of free-radical intermediates in some reactions involving periodate. J Chem Soc 2794–2796

Turbak AF, Snyder FW, Sandberg KR (1983) Microfibrillated cellulose, a new cellulose product: properties, uses, and commercial potential. J Appl Polym Sci Appl Polym Symp 37:815–827

Varma AJ, Chavan VB, Rajmohanan PR, Ganapathy S (1997) Some observations on the high-resolution solid-state CP-MAS carbon-13 NMR spectra of periodate-oxidized cellulose. Polym Degrad Stab 58:257–260

Yang H, Alam MN, van de Wen TGM (2013) Highly charged nanocrystalline cellulose and dicarboxylated cellulose from periodate and chlorite oxidized cellulose fibers. Cellulose 20:1865–1875

Zeronian SH, Hudson FL, Peters RH (1964) The mechanical properties of paper made from periodate oxycellulose pulp and from the same pulp after reduction with borohydride. Tappi 47:557–564

Zhang J, Jiang N, Dang Z, Elder TJ, Ragauskas AJ (2008) Oxidation and sulfonation of cellulosics. Cellulose 15:489–496

Zhao H, Heindel ND (1991) Determination of degree of substitution of formyl groups in polyaldehyde dextran by the hydroxylamine hydrochloride method. Pharm Res 8:400–402